Evaluation of Particle Resuspension and Single-layer Rates with Exposure Time and Friction Velocity for Multilayer Deposits in a Turbulent Boundary Layer

Sofia Eirini Chatoutsidou, Mihalis Lazaridis[*]

School of Environmental Engineering, Technical University of Crete, 73100 Chania, Greece

ABSTRACT

The present work deals with the resuspension of small nondeformable particles from multilayer deposits in a turbulent boundary layer. A kinetic force-balance approach was adopted to model particle motion at the point of detachment, whereby intermolecular interactions were modeled by the Lennard-Jones potential. The rate of change of the number of particles was estimated for each discrete layer based on existing kinetic models. In particular, the kinetic equations of Lazaridis and Drossinos (1998), *LD*, and Friess and Yadigaroglu (2001), *FY*, were implemented and compared using lattice arranged deposits. The influence of exposure time and friction velocity was investigated through the obtained resuspension rates. It was found that the single-layer resuspension rates were substantially affected by the layer position within the deposit as well as considerably influenced by both the exposure time and the friction velocity. Moreover, the numerical results demonstrate that the *LD* kinetic estimates higher resuspension rates compared to the *FY* kinetic only for short exposures to the flow, predominantly due to a different expression for the fraction of exposed particles. In addition, the present study recognized the time dependence (i.e., a short-term vs. long-term regime) of the resuspension rate observed both experimentally (Wu *et al.*, 1992; Wang *et al.*, 2012) and by model predictions (Lazaridis and Drossinos, 1998; Friess and Yadigaroglu, 2001; Reeks and Hall, 2001) and confirmed the inverse dependence of the resuspension rate with time in long-term regime. Two regimes were also identified while evaluating the resuspension rate for a range of friction velocities, viz., a low-friction regime in which the resuspension rate increases with friction and a high-friction regime in which the opposite behaviour was observed.

Keywords: Multilayer deposit; Resuspension; Kinetics; Adhesion.

NOMENCLATURE

Symbol

A	Hamaker constant.
$f_R(t)$	fraction of remaining particles (averaged).
$\overline{f^2}$	mean square of the fluctuating removal force.
$\dot{f^2}$	time derivative of f^2.
J	single-layer resuspension rate constant.
k	number of layers.
m	particle mass.
N	number of particles in each layer.
N_i	number of particles in layer i at time t.
n_i	number density.
$p_i(t)$	fraction of remaining particles.
Q	height of the potential well.
R_p	particle radius.
R^+	dimensionless particle radius.
R_{eff}	effective particle radius.

R'	normalized particle radius.
$\overline{R}'$	geometric mean of R'
r_{eq}	particle position at equilibrium.
r_{det}	position of particle detachment.
r	distance between the particle and the substrate or distance between two spheres.
t	time.
U	average potential energy of particle.
u_*	friction velocity.
$V(r)$	Lennard-Jones potential energy.
v_f	fluid kinematic viscosity.
y^2	mean square displacement.

Greek

δ	distance between asperities.
ε	decay constant.
ε_{12}	geometric mean of Lennard-Jones parameters.
$\Lambda(t)$	fractional resuspension rate.
ρ_f	fluid density.
σ_a	standard deviation.
σ_{12}	arithmetic mean of Lennard-Jones parameters.
ω_0	frequency of particle in the potential well.
ω_p	natural frequency of vibration of the bound particle.

[*] Corresponding author.
  E-mail address: lazaridi@mred.tuc.gr

INTRODUCTION

Particle resuspension from surfaces involves the physical process at which particles are detached from a surface and remain suspended into the ambient environment. The term denotes that prior to detachment particles were firstly deposited onto the surface but under the influence of an external force resuspension occurred. Therefore, resuspension depends substantially on the morphology of the deposit that can be either monolayer or multilayer (Boor *et al.*, 2013b). A monolayer deposit consists of a single layer of particles adhered on top of a surface, whereas, a multilayer deposit includes several layers of particles sit on top of other particles above a surface.

Resuspension and re-entrainment of particles has important impact on air quality (Zhou *et al.*, 2011; Boor *et al.*, 2013a) and thus on human exposure to harmful contaminants. Particle resuspension induced by a turbulent airflow has been studied extensively due to its implication in nuclear industry, wind tunnel applications or even human-induced activities (Wu *et al.*, 1992; Ziskind *et al.*, 2006; Stempniewich *et al.*, 2008; Mukai *et al.*, 2009; Herny and Minier, 2014). As a first step, monolayer resuspension was studied thoroughly both by experimental studies and theoretical models. Particle size, airflow characteristics, surface roughness and adhesive forces were identified as factors that influence particle resuspension. In particular, it was demonstrated that particle motion is initiated by the creation of torque upon the particle and rolling is the dominant resuspension mechanism causing particle detachment for small particles fully immersed into the viscous sublayer (Ziskind *et al.*, 1995; Henry and Minier, 2014; Chatoutsidou *et al.*, 2017). In addition, studies have shown that the distribution of particle size, statistical variation of the surface roughness and their impact to adhesive forces as well as material properties influence resuspension characteristics leading to a variety of experimental observations (Reeks and Hall, 2001; Ibrahim *et al.*, 2003; Guingo and Minier, 2008; Goldasteh *et al.*, 2013; Chatoutsidou *et al.*, 2017). These observations give evidence that particle resuspension is a complex process where particle motion and its eventual entrainment to the ambient air is determined by statistical characteristics of the factors involved.

Resuspension from multilayer deposits, on the other hand, has received less attraction due to the difficulty of investigating the process itself. Though, it is equally important since particles are easily found in multilayer deposits in real environments (Boor *et al.*, 2013). Recent research however focused on particle behaviour in multilayer deposits, resuspension kinetics and investigation of its characteristics (Barth *et al.*, 2013; Zhang *et al.*, 2013; Lecrivain *et al.*, 2014). Unlike monolayer resuspension, particle entrainment to the airflow from a multilayer deposit leads to uncovering a particle lying underneath, thus resuspension moves deeper in the deposit. This intrinsic characteristic makes evolution of multilayer resuspension a demanding process regarding modeling of the structure of the deposit, intra-layer interactions and particle-fluid interactions. It is well established by now that morphology of the deposit plays an important role on multilayer resuspension (Henry and Minier, 2014). In that sense, layer position in the deposit as well as particle arrangement is of major importance when dealing with resuspension rates.

A first attempt to model multilayer resuspension is presented in the work done by Fromentin (1989), whereby a semi-empirical model based on a force-balance (adhesive vs. aerodynamic forces) method is used to predict the resuspension flux. Later, Lazaridis and Drossinos (1998) and Friess and Yadigaroglu (2001) proposed a set of coupled kinetic equations to estimate the resuspension rates. Both studies used a lattice structure for the deposit where the resuspension rate is driven by the rate of change of the number of particles in each layer. Particles were assumed to detach one by one, a limitation that was outreached in a subsequent work done by Friess and Yadigaroglu (2002) where particle resuspension from clusters was examined along with the impact from the porosity of the deposit. Indeed, it is evident that particles from multilayer deposits are likely resuspended in clusters rather than sole entities (Barth *et al.*, 2013; Lecrivain *et al.*, 2014). Recently, Zhang *et al.* (2013) used a hybrid resuspension model to investigate, among others, the impact of layer coverage and particle size distribution to multilayer resuspension.

The present model assumes a simplified deposit of particles, where particles sit on top of other particles and a turbulent airflow acting upon them. The particles are considered small enough to be immersed into the viscous sublayer of the turbulent boundary layer, where particle resuspension is induced due to rolling. A kinetic force-balance approach similar to Chatoutsidou *et al.* (2017) was followed to determine the resuspension rate for each discrete layer. Single-layer kinetics were obtained using the kinetics proposed by Lazaridis and Drossinos (1998) and Friess and Yadigaroglu (2001). The objective was to investigate the impact of exposure time and friction velocity in a resuspension event in respect to layer position into the deposit. The *LD* and *FY* kinetics were examined in order to investigate the impact of both kinetics to the resuspension rate.

MULTILAYER RESUSPENSION MODEL

Deposit Structure and Particle Resuspension Mechanism

As recent studies evidence (Zhang *et al.*, 2013; Henry and Minier, 2014), the importance of the morphology of the deposit is a major factor on investigating key elements of the process. Fig. 1(a) presents a simplified lattice deposit that was originally used by Lazaridis and Drossinos (1988) and Friess and Yadigaroglu (2001) to investigate the characteristics of multilayer resuspension. Significant improvement of the structure of the deposit can be found in literature by now, such as particles sitting on the hole created between two particles from the layer beneath, introducing a distribution of particle size, porosity of the deposit, coverage effect (Friess and Yadigaroglu, 2002; Zhang *et al.*, 2013). Different structures may lead to quantitative analysis for the resuspension rates and particle behaviour within the deposit, however fundamental issues such as

particle resuspension as clusters still remains unsolved.

The present model considers a multilayer deposit of small nondeformable particles on a flat substrate and a turbulent airflow acting upon the deposit. An idealized deposit as the one used by Lazaridis and Drossinos (1988) and Friess and Yadigaroglu (2001) was chosen to model particle resuspension. Accordingly, k layers of the same identical particles are stacked on top of others, therefore, particles sit on top of other particles or on the flat substrate (bottom layer). The number of particles N in each discrete layer was assumed the same and only the physical interactions between particles at different layers were considered.

Particle motion arising from the impact of the airflow determines the resuspension mechanism. This study considers that the airflow acts upon the particles, which are small enough to lie into the viscous sublayer of the turbulent boundary layer. Studies on monolayer deposits have shown that in this case rolling is the dominant resuspension mechanism with the lift and drag forces exerted on the particle creating a moment that causes particle detachment and re-entrainment to the flow (Ziskind *et al.*, 1997; Ibrahim *et al.*, 2003; Reeks and Hall, 2001; Guingo *et al.*, 2008; Chatoutsidou *et al.*, 2017).

Considering a particle that rests between two asperities due to microscale roughness of the underlying surface, the total couple generated by a two-point contact and the resulting effective force are given respectively (Chatoutsidou *et al.*, 2017):

$$\Gamma = \frac{\delta}{2}F_l + R_p F_d \Leftrightarrow F = \frac{1}{2}F_l + \frac{R_p}{\delta}F_d, \tag{1}$$

where δ is the distance between the asperities and R_p/δ is the geometric factor. The latter represents the ratio of the tangential to the normal force and was assumed with a value of 100 (Reeks and Hall, 2001). The mean aerodynamic lift and drag forces were estimated respectively by Leighton and Acrivos (1985) and O'Neill (1968):

$$F_l = 9.22\rho_f v_f^2 \left(R^+\right)^4, \quad F_d = 1.72 : \pi\rho_f u_*^2 R_p^2 \tag{2}$$

where ρ_f is the fluid density, v_f the fluid kinematic viscosity, u_* is the friction velocity and R^+ is the dimensionless particle radius ($R^+ = R_p u_*/v_f$).

Kinetics of a Multilayer Deposit

Given a simplified deposit as the one shown in Fig. 1(a), a kinetic to describe the time evolution of a multilayer deposit was originally given by Lazaridis and Drossinos (1998), followed subsequently by the kinetic proposed by Friess and Yadigaroglu (2001). Both kinetics use a set of coupled equations that describe the rate of change of the number of particles in layer i. Accordingly, for $i > 2$ the two kinetics provide:

$$\frac{dN_i}{dt} = -JN_i\left[1 - \frac{N_{i-1}(t)}{N_{i-1}(0)}\right], \quad (\text{LD}) \tag{3}$$

$$\frac{dN_i}{dt} = -JN_i\left[1 - \frac{N_{i-1}(t)}{N_i(t)}\right], \quad (\text{FY}) \tag{4}$$

where N_i is the number of particles in layer i at time t, J is the single-layer resuspension rate constant and 0 denotes the initial number of particles in a given layer. As far as for $i = 1$, the layer exposed to the flow, the rate of change of the number of particles is given by a simple first-order kinetic equation (Reeks *et al.*, 1988):

$$\frac{dN_1}{dt} = -JN_1 \tag{5}$$

Eqs. (3) and (4) indicate that both models provide the rate of change of N_i with the same expression but altering the quantity in the parenthesis, namely the fraction of
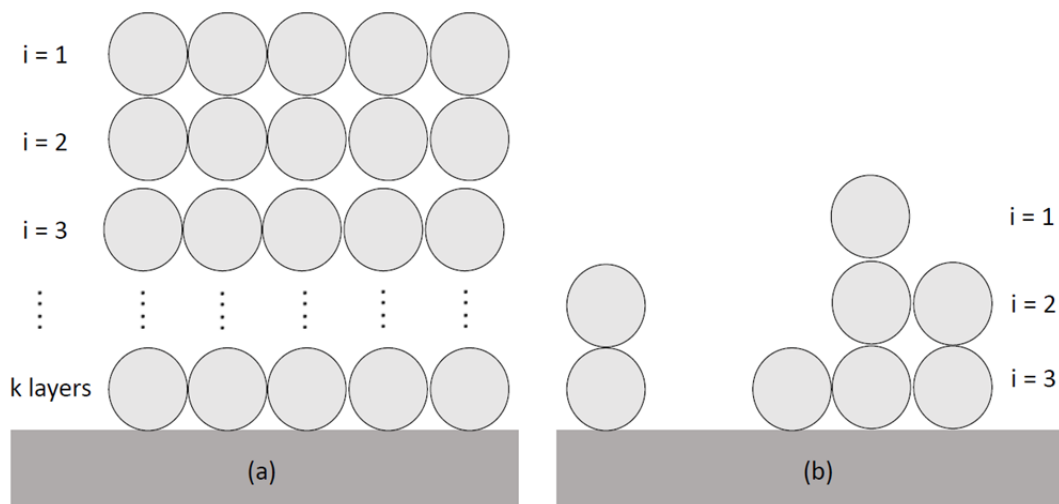
Fig. 1. Geometry of the lattice deposit: (a) generalized deposit with k layers and (b) a 3-layer deposit with randomly resuspended particles.

exposed particles to the flow. The *LD* kinetic determines the fraction of exposed particles at i^{th} layer as the fraction of particles that was removed from the layer above $(i − 1)$ at time t. On the other hand, the *FY* kinetic determines the fraction of exposed particles as the ratio of the particles in $(i − 1)^{th}$ layer to the particles at i^{th} layer at time t. As such the *LD* kinetic provides the maximum resuspension rate since it includes the initial number of particles at the $(i − 1)$ layer in the expression for the fraction of exposed particles, which in the present case is equal to N. On the contrary, the *FY* kinetic provides the fraction of exposed particles at the exact time t. Intrinsically, this difference makes the *FY* kinetic linear and the kinetic equations can be solved analytically, whereas, the *LD* kinetic is not linear and only the first three equations were provided by the authors.

Table 1 presents an example of the fraction of exposed particles as it was calculated for both kinetics based on the geometry presented in Fig. 1(b). It is demonstrated that the *LD* kinetic calculates significantly higher fraction of exposed particles for both cases as a direct consequence of using the initial number of particles in the denominator for both layers, the reason beneath the *LD* kinetic is believed to provide with the maximum resuspension rates.

The Lennard-Jones Intermolecular Potential

Intermolecular interactions in the present model involve two cases: interactions between particles at different layers (particle-particle) and interactions between particles and a plane surface (particle-surface). In addition, particles were considered hard with no deformation, therefore, any effect from elastic flattening was neglected.

Interaction Potential for a Particle-surface System

Integration of the Lennard-Jones potential between a smooth sphere with particle radius R_p which is in contact with a plane surface provides the energy for a particle-surface interaction (Lazaridis *et al.*, 1998):

$$V_{sp}(r) = -\frac{A}{6}C_a + BC_b, \tag{6}$$

where,

$$A = \pi^2 C n_1 n_2, \; B = \frac{A}{45}\sigma_{12}^6, \; C = 4\varepsilon_{12}\sigma_{12}^6, \tag{7}$$

$$C_a = \frac{2R_p(R_p + r)}{r(2R_p + r)} + \ln\left(\frac{r}{2R_p + r}\right),$$

$$C_b = \frac{1}{168}\left[\frac{1}{(r + 2R_p)^6} - \frac{1}{r^6}\right] + \frac{R_p}{28}\left[\frac{1}{(r + 2R_p)^7} - \frac{1}{7}\right],$$

where A is the Hamaker constant, r is the distance between the surface of the particle and the substrate surface and n_i is the number density of molecules in the solid j. The parameters ε_{12} and σ_{12} are estimated by the arithmetic, $\sigma_{12} = (\sigma_1 + \sigma_2)/2$ and the geometric, $\varepsilon_{12} = (\varepsilon_1\varepsilon_2)^{1/2}$ mean of the single-species parameters.

Interaction Potential for a Particle-particle System

The interaction energy between two identical spheres of radius R_p in contact is written (Lazaridis and Drossinos, 1998):

$$V_{PP}(r) = -\frac{A}{6}C_c + \frac{9B}{C_1}C_d, \tag{8}$$

with,

$$C_1 = 2R_p + r$$

$$C_c = \frac{2R_p^2}{C_1^2} + \frac{2R_p^2}{C_1^2 - 4R_p^2} + \ln\frac{C_1^2 - 4R_p^2}{C_1^2},$$

$$C_d = \frac{C_7}{3528} + \frac{C_8}{72} + \frac{C_6}{1296} + \frac{C_5}{360},$$

$$C_7 = \frac{224R_p^2 - 14C_1^2}{C_1^7} + \frac{7C_1^2 - 112R_p^2 - 98C_1R_p}{(C_1 + 2R_p)^7} + \frac{7C_1^2 - 112R_p^2 + 98C_1R_p}{(C_1 - 2R_p)^7},$$

$$C_8 = \frac{2C_1R_p^2 - R_pC_1^2}{(C_1 - 2R_p)^8} + \frac{2C_1R_p^2 + R_pC_1^2}{(C_1 + 2R_p)^8} - \frac{4R_p^2}{C_1^7},$$

$$C_6 = \frac{12}{C_1^5} - \frac{6C_1 + 18R_p}{(C_1 - 2R_p)^6},$$

$$C_5 = -\frac{2}{C_1^5} + \frac{1}{(C_1 + 2R_p)^5} + \frac{1}{(C_1 - 2R_p)^5},$$

where A and B represent the same properties as in Eq. (7) and r is the distance between the two spheres.

Table 1. Calculated fraction of exposed particles for layer 2 and 3 using the geometry in Fig. 1(b). Comparison between the *LD* and *FY* kinetics.

Kinetic	Layer 2	Layer 3
Lazaridis and Drossinos (1998)	$1 - \frac{1}{5} = 0.8$	$1 - \frac{3}{5} = 0.4$
Friess and Yadigaroglu (2001)	$1 - \frac{1}{3} = 0.67$	$1 - \frac{3}{4} = 0.25$

Single-layer Resuspension Rate Constant

The single-layer resuspension rate constant was approximated by the same methodology as presented in Chatoutsidou *et al.* (2017), based predominantly in the work of Reeks *et al.* (1988). Accordingly, *J* is given as:

$$J = \omega_0 exp\left(-\frac{Q}{2U}\right), \tag{9}$$

where ω_0 is the typical forcing frequency of the particle in the potential well, Q is the height of the potential well at particle detachment point with respect to the particle equilibrium position and U is the average potential energy of the particle in the potential well. In the present work, *J* was chosen to be expressed by potential differences as shown in Eq. (9), where the resonant energy transfer was neglected. Hence, a force balance approach was used where the bound particle resuspends when the instantaneous aerodynamic forces (lift and drag) exceed the total adhesive forces of the interaction system.

Following the work of Zhang *et al.* (2013), ω_0 is estimated as:

$$\omega_0 = \frac{1}{2\pi}\left[\frac{\dot{f}^2}{f^2}\right]^{1/2} = \frac{0.1642}{2\pi}\left(\frac{u_*^2}{v_f}\right) \tag{10}$$

where f^2 is the mean square of the fluctuating removal force and $\dot{f}^2$ its time derivative.

The potential barrier *Q* was estimated numerically by the difference of the potential energy between the equilibrium point (minimum energy) and the energy at the detachment point. The detachment point was determined by finding where the total force acting on the particle was zero. The potential barrier is written as:

$$Q = V(r_{det}) - V(r_{eq}) \tag{11}$$

where r_{det} is the position of particle detachment, and r_{eq} the particle position at equilibrium. $V(r)$ corresponds either to the particle-particle potential, $V_{pp}(r)$, or to the particle-surface potential, $V_{sp}(r)$.

The average potential energy for a harmonic oscillator is given:

$$U = \frac{1}{2}m\omega_p^2 y^2 \tag{12}$$

where *m* is the particle mass, ω_p is the natural frequency of vibration of the bound particle and y^2 is the mean square displacement estimated by $y^2 = f^2/m^2\omega_p^4$. The fluctuating part of the aerodynamic force $\sqrt{f^2}$ was assumed as 0.366 of the aerodynamic removal mean force (Zhang *et al.*, 2013), whilst ω_p was estimated by:

$$\omega_p = \left[\frac{1}{m}\frac{d^2V(r)}{dr^2}\right]^{1/2}_{eq} \tag{13}$$

Eq. (13) was evaluated at equilibrium where the interaction energy is minimum and corresponds to the distance of the closest approach. The distance of closest approach was determined from the zero of the first derivate of the total potential ($dV(r)/dr = 0$).

Note that in the present work *J* depends explicitly on the interaction system or equivalently to the position of the layer in the deposit. The single-layer resuspension rate constant may be estimated using the potential differences provided by Eq. (6), when the interaction potential involves a particle-surface interaction or by using Eq. (8) when the interaction potential involves a particle-particle interaction. In other words, layers that include only particle interactions are characterized by the same J_{pp}, whereas, only the bottom layer of the deposit includes particle-surface interactions thus characterized by a different J_{sp}. Both Friess and Yadigaroglu (2001) and Zhang *et al.* (2013) estimate *J* independently of the position of the layer, a differentiation that has impact in the present model.

Adhesive Force Distribution

The reduced adhesive force due to surface roughness was modeled introducing an adhesive force distribution via a log-normal probability density function. Assuming an effective particle radius R_{eff} which corresponds to the reduced adhesive force, the normalized particle radius is defined as $R' = R_{eff}/R_p$ and the probability density function is written as (Lazaridis *et al.*, 1998; Chatoutsidou *et al.*, 2017):

$$\phi(R')dR' =$$
$$\frac{1}{(2\pi)^{1/2}\ln\sigma_a}exp\left\{-\frac{1}{2(\ln\sigma_a)^2}\left[\ln\frac{R'}{\overline{R}'}\right]^2\right\}d(\ln R') \tag{14}$$

where, $\overline{R}'$ is the geometric mean of R' representing the reduction in adhesion forces and σ_a is the standard deviation representing the spread in adhesion forces. Both variables have significant influence on the resulting adhesive force distribution: Higher reduction results in substantially reduced adhesive forces thus easier resuspension, whilst, higher spread implies a broader distribution of adhesive forces and the surface exhibits significant variability of concavities. In lack of experimental data to evaluate model predictions, previously implemented values were chosen for the two variables, i.e., the reduction was set equal to 1000 and the spread was set equal to 2 for all simulations (Chatoutsidou *et al.*, 2017)

The fraction of remaining particles $f_R(t)$ after exposure to flow for time *t* was obtained by averaging over the log-normal distribution, whilst the fractional resuspension rate $\Lambda(t)$ was estimated by the negative first derivative of $f_R(t)$ (Reeks *et al.*, 1988; Lazaridis *et al.*, 1998). The equations read respectively:

$$f_R(t) = \int_0^\infty exp[-J(R')t]\phi(R')dR', \tag{15}$$

$$\Lambda(t) = -\frac{df_R(t)}{dt}. \tag{16}$$

RESULTS AND DISCUSSION

Assessment of Particle-particle and Particle-surface Interactions

Since particle resuspension is determined by the balance of forces that are required to entrain the particle to the ambient air and those that adhere the particles on the surface, an assessment of the interactions used in the present model becomes essential. Fig. 2 plots the fraction of remaining particles against friction velocity for a resuspension event including a case of particle-particle interaction and a case of particle-surface interaction.

The assessment is presented in the aspect of resuspension of a layer of particles (top layer) which are deposited either on a layer of the same particles or on a plane surface. The surface and the particles were chosen of the same compound for comparable results. Accordingly, the resuspension kinetic involves the same top layer kinetic but different approximations of the interaction potential were used due to different intermolecular interactions.

Fig. 2 demonstrates that the stainless steel particles are detached at lower friction velocity when the layer below corresponds to the same particles, whereas, higher friction is required to detach the same amount of particles when the layer below corresponds to a stainless steel surface. This finding is directly associated with the interaction potential that was used in each case and by extend to the adhesive force. Since, the only difference lies in the inclusion of the interaction potential, it is concluded that the adhesive force for a particle-surface interaction is stronger than the adhesive force between two layers of the same particles. Thus, it is easier for a particle to resuspend when it rests on top of other particles than on top of a surface. The present finding is in agreement with Lazaridis and Drossinos (1998), where the authors simulated the interaction potential between two identical particles and between a particle and a surface and proposed that higher energy is required to overcome the threshold energy at equilibrium of a particle-surface interaction.

Comparison of the LD and FY Kinetics

A comparison of model predictions between the *LD* and the *FY* kinetics is shown in Fig. 3, where the fraction of remaining particles and the fractional resuspension rate are plotted versus time. The results correspond to the second (particle-particle) and third (particle-surface) layer of a 3-layer deposit. Model implementation for the second layer involves the condition $J_2 = J_1$ due to only particle interactions between layers 2 and 3. However, layer 3 involves a particle-surface interaction potential, thus, $J_3 \neq J_2$. The equations used for each layer are written respectively:

$$\text{Layer 2: } p_2(t) = \exp\left[-J_1 t - \left(e^{-J_1 t} + 1\right)\right], \; (LD)$$

$$p_2(t) = e^{-J_1 t}\left(1 + J_1 t\right), \; (FY)$$

$$\text{Layer 3: } p_3(t) = \exp\left[-J_3 t - \frac{J_3}{J_1} e^{\left(1 - e^{-J_1 t}\right)} - \frac{J_3}{J_1}\right], \; (LD)$$

$$p_3(t) = e^{-J_3 t}\left[1 - \frac{J_3}{J_3 - J_1} + \frac{J_3 J_1}{\left(J_3 - J_1\right)^2}\right]$$
$$+ e^{-J_1 t}\left[\frac{J_3}{J_3 - J_1}\left(1 + J_1 t\right) - \frac{J_3 J_1}{\left(J_3 - J_1\right)^2}\right], \; (FY)$$

According to Fig. 3(a) the fraction of remaining particles in both layers is similar, although slightly higher values were obtained by the *FY* kinetic. Model predictions suggest
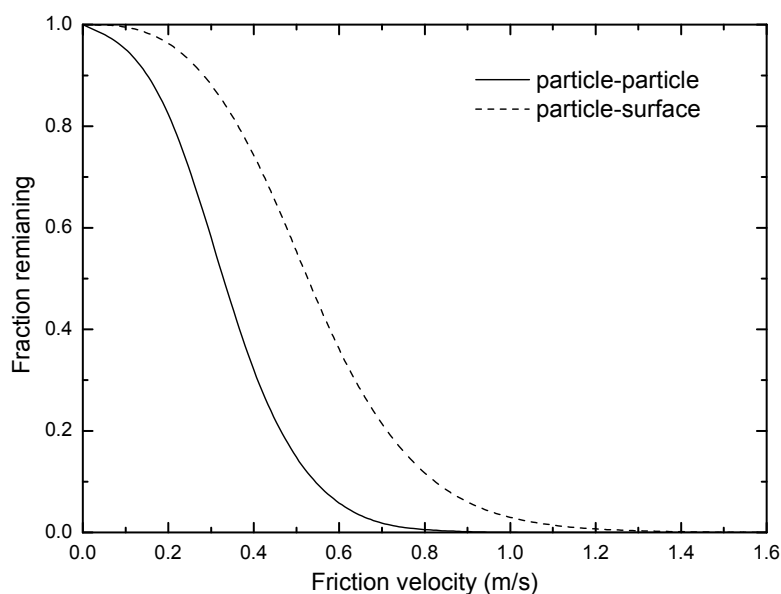
Fig. 2. Fraction remaining of a top layer of 70 μm stainless steel particles versus friction velocity. Top layer interactions were modeled for particles resting on top of the same particles (particle-particle) or on top of a surface (particle-surface).
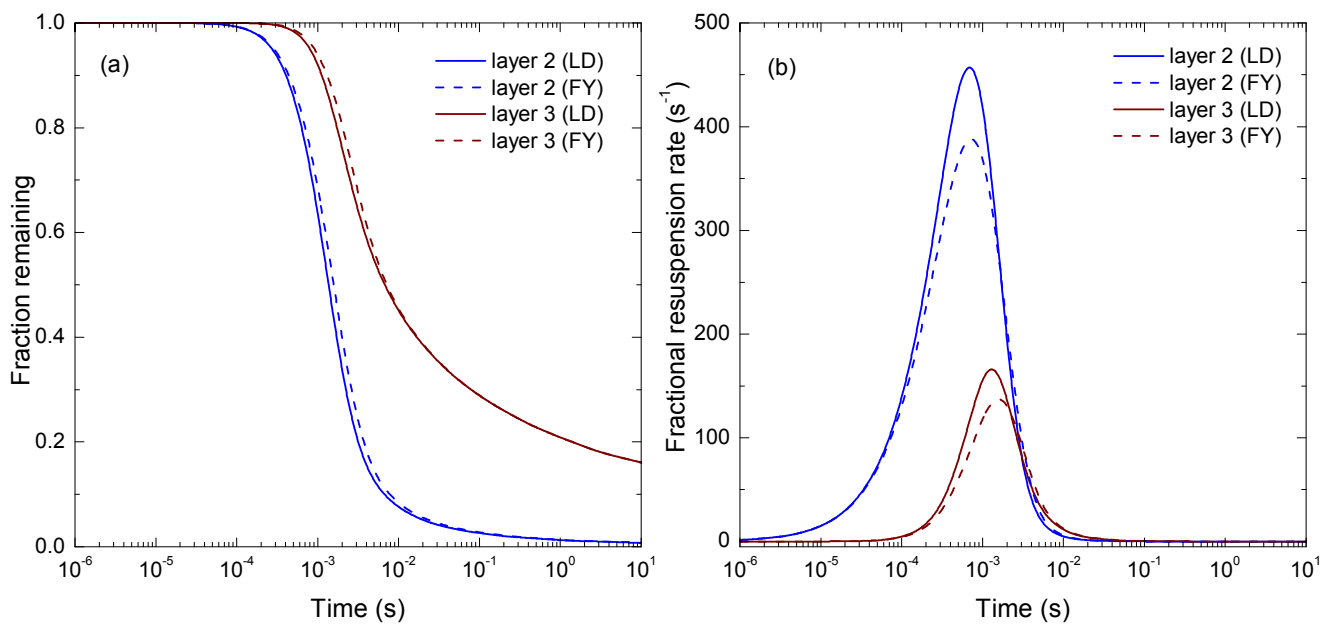
Fig. 3. Comparison between the *LD* and *FY* kinetics for the second and the third layer of a 3-layer deposit of 30 μm stainless steel particles on a stainless steel surface at friction velocity 1 m s^{-1}: (a) fraction remaining and (b) fractional resuspension rate Λ(*t*) versus time.

that the *LD* kinetic estimates less particles remaining on the surface, compared to the *FY* kinetic, for the same exposure time. In addition, Fig. 3(b) indicates that the *LD* kinetic calculates rates higher than the *FY* kinetic at short exposure time. Indeed, the fractional resuspension rate Λ(*t*) is higher while using the *LD* kinetic for exposure time < 10^{-3} s, whilst similar rates apply for both kinetics at longer exposure to the flow. These results strongly suggest that the exposure time to the flow plays an important role on the differences that may arise between the two kinetics.

Furthermore, a comparison between the *LD* and *FY* kinetics at different friction is given in Fig. 4. Fig. 4(a) demonstrates that both kinetics estimate the same fraction of remaining particles for layer 2 and layer 3, with the curves being identical at exposure time 1 s. However, at shorter exposure time (10^{-3} s, Fig. 4(b)) the *LD* kinetic produces lower values for the fraction of remaining particles for both layers. This finding suggests that higher rates apply for the *LD* kinetic for short exposure to the flow (in agreement with Fig. 3(b)) and that the exposure time is essentially the key factor that determines the difference between the *LD* and FY kinetics. Unlike exposure time, no impact of friction velocity was found while comparing the two kinetics.

Resuspension from Multiple Layers

Fig. 5 presents the results of the model applied to a 5-layer deposit using the *FY* kinetic. Layer 1 corresponds to the layer exposed to the flow (top layer) and particle-particle interactions were used. Similarly, particle-particle interactions were used for layers 2 to 4. On the other hand, layer 5 corresponds to the bottom layer, thus, the interaction potential was modeled using particle-surface interactions.

Model simulations for the fraction of remaining particles suggest that the top layer (layer 1) resuspends first, followed by the resuspension of the rest of the layers according to their position in the deposit. In reality, the conditions for detachment require the direct contact of the particle with the external force, herein the airflow. The particle in judgment is considered possible for resuspension when it is unobstructed from above, e.g., the particle is exposed to the flow. This hypothesis was adopted into the model by considering a particle lying within the deposit capable for resuspension only under the condition of an unoccupied position above it. The same methodology was adopted in Friess and Yadigaroglou (2002) and Lecrivain *et al.* (2014). Therefore, layers located closer to the top layer resuspend prior to layers located further into the deposit.

Moreover, Fig. 5 indicates a difference in the fraction remaining of layer 5 between the examined friction velocities. It is observed that after 10^3 s exposure to the flow, layers 1–4 are completely resuspended, in contrast with layer 5 where the fraction of remaining particles is 0.4 at *u*∗ = 0.5 m s^{-1} but reaches a zero value at *u*∗ = 1 m s^{-1}. The higher fraction of remaining particles found for layer 5 at *u*∗ = 0.5 m s^{-1} is attributed to the adhesive force. The present results propose that the particles in layer 5 bind on the surface with stronger adhesive force as a direct consequence of the interaction potential that was used to model the particle-surface interactions. As a result, higher external force (friction) is required to detach more particles from layer 5, whereas longest exposure time to the flow will not cause more particles to resuspend. Therefore, at *u*∗ = 1 m s^{-1} where the removal force is stronger, layer 5 resuspends completely (along with the rest of the layers). This finding demonstrates the implications originated from the two interaction potentials that were implemented in the present study and its impact to the numerical results.

Moreover, a simultaneous comparison of the results in
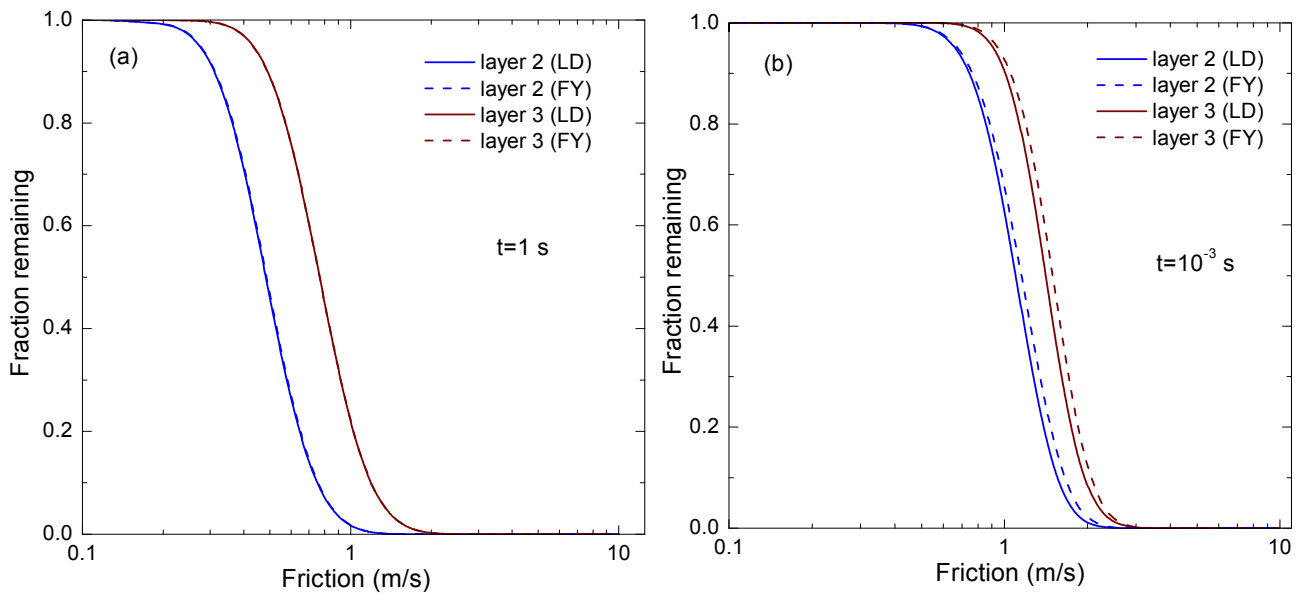
Fig. 4. Fraction remaining of 30 μm stainless steel particles on a stainless steel surface versus friction velocity. Comparison between the *LD* and *FY* kinetics for the second and the third layer (of a 3-layer deposit) at: (a) exposure time 1 s and (b) exposure time 10^{-3} s.
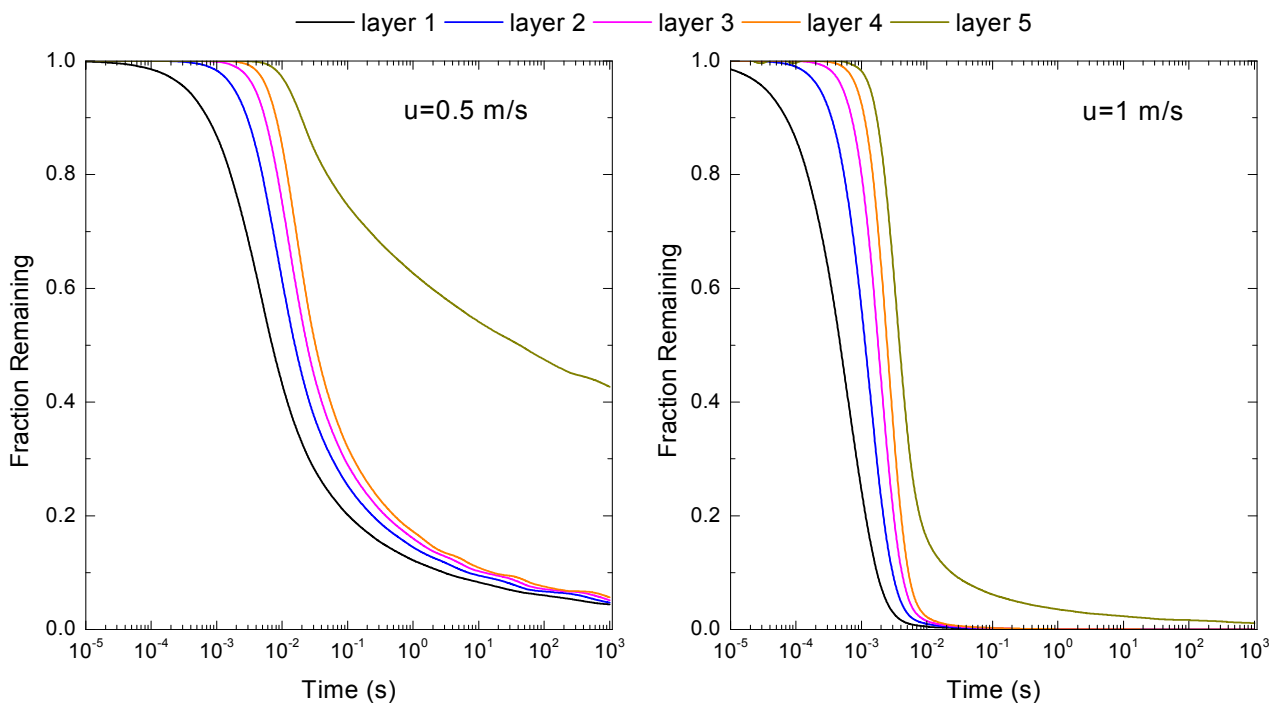
Fig. 5. Fraction remaining of 60 μm stainless steel particles on a stainless steel surface versus time for each layer of a 5-layer deposit. Comparison of model predictions between two friction velocities. The *FY* kinetic was used.

Figs. 4(a) and 5(b) demonstrates the easier detachment for larger particles. Particle size plays important role on resuspension with smaller particles exhibit significantly lower external force compared to a larger particle (Eq. (2)), thus, in Fig. 4(a) the fraction remaining for $u = 0.5$ m s^{-1} and $t = 1$ *s* for layer 2 (FY) is 0.48 for 30 micron particles whereas Fig. 5(a) indicates that the fraction remaining for 60 micron particles in layer 2 (FY) at $t = 1$ *s* and $u = 0.5$ m s^{-1} is 0.14.

The fractional resuspension rate $\Lambda(t)$ obtained for each layer of a 5-layer deposit is shown in Fig. 6. The (top) layer 1 resuspends first and is characterized by the highest rates. Accordingly, all particles at the top layer are unobstructed from above thus free to resuspend as long as it is stochastically possible. However, $\Lambda(t)$ for the layers beneath are substantially dependent on the layer above them, therefore, a different behaviour is observed where
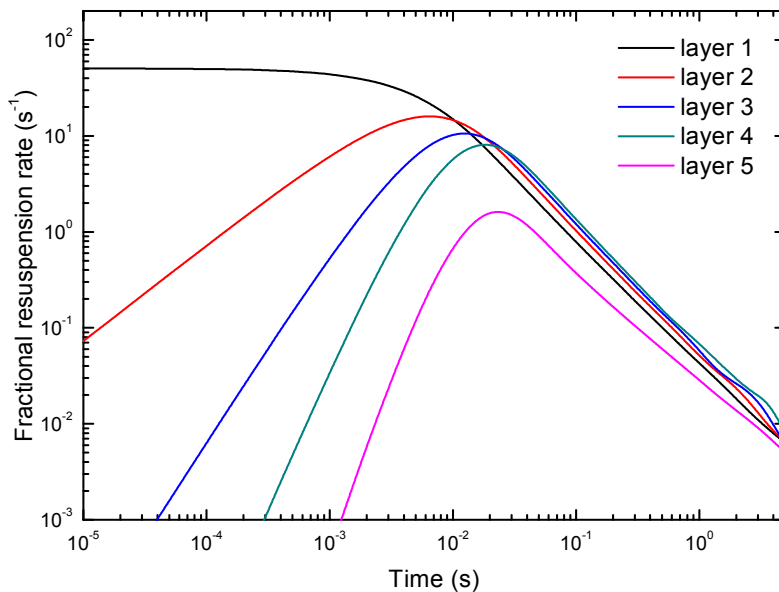
Fig. 6. Fractional resuspension rate for each layer of a 5-layer deposit of 60 stainless steel particles on a stainless steel surface versus time at friction 0.4 m s^{-1}. The *FY* kinetic was used.

$\Lambda(t)$ increases with time. This increase of $\Lambda(t)$ for $t < 10^{-2}$ s is associated with more particles detached from each layer as exposure time increases. As long as the number of detached particles increases from the top layer, the exposed particles at the second layer become more and the resuspension rate increases with time. Accordingly, the same condition applies for particles at layer 3, 4 and 5. Thus, $\Lambda(t)$ at short exposure to the airflow is lower for higher layer number: particles at layers $i \geq 2$ require a short-time period in order to be uncovered. In general, for a thicker deposit it is expected that $\Lambda(t)$ preserves lower rates for higher layer number. Similar findings are reported in Zhang *et al.* (2013).

Additionally, Fig. 7 presents the total fractional resuspension rate for 3 deposits that differ only in the number of layers. For all three cases $\Lambda(t)$ presents similar rates at a very short exposure time but as t increases $\Lambda(t)$ follows different rates for different deposits. This observation is directly linked with the growth of resuspension within the deposit. At $t < 3 \times 10^{-3}$ *s* resuspension takes place only at the first three layers for all deposits, thus $\Lambda(t)$ preserves similar rates. However, as resuspension moves further into the deposit particles start to detach from layer 4 and $\Lambda(t)$ retains high values for the 5-layer and the 10-layer deposit. On the contrary, $\Lambda(t)$ for the 3-layer deposit (no 4th layer) decreases. The same finding applies for the 5-layer deposit, thus at $t = 10^{-2}$ particle resuspension starts to take place at layer 6 of the 10-layer deposit and the deviation between the two curves is observed. These results match the ones presented by Zhang *et al.* (2013) and strongly suggest that the fractional resuspension rate preserves higher values as the number of layer increases, i.e., when thicker deposits are involved.

Influence of Exposure Time and the 1/t Law

Both Figs. 6 and 7 demonstrate a relationship of the fractional resuspension rate $\Lambda(t)$ with exposure time to the

flow. Accordingly, two regimes are identified: a short-term regime ($< 10^{-2}$ s) where the resuspension rate is high and a long-term regime ($> 10^{-2}$ s), where the resuspension rate decays algebraically with time. Our numerical results are in agreement with previous studies (Reeks *et al.*, 1988; Lazaridis and Drossinos, 1998; Reeks and Hall, 2001; Friess and Yadigaroglu, 2002), where the long-term resuspension rate was found to depend inversely with exposure time. This behaviour is strongly associated with the balance of adhesive and aerodynamic forces (Reeks *et al.*, 1988; Friess and Yadigaroglu, 2001; Benito *et al.*, 2015). At small timescales where the low adhered particles are instantaneously resuspended, the aerodynamic forces are stronger than the adhesive forces and high rates are observed. However, at higher exposure time the fraction of strongly adhered particles on the surface increases and the resuspension rate decreases considerably.

Theoretical predictions (Wen and Kasper, 1989; Reeks *et al.*, 1988; Lazaridis *et al.*, 1998; Reeks and Hall, 2001; Friess and Yadigaroglu, 2002) associate the long-term fractional resuspension rate with the inversely dependence on the exposure time. Indeed, $\Lambda(t)$ decreases linearly with exposure time after a short period corresponding to the short-term regime. The power law that determines the decay of the resuspension rate is in the form:

$$\Lambda(t) = constant\ t^{-\varepsilon} \qquad (17)$$

where, ε represents the decay constant. Several authors have suggested that ε corresponds to values close to 1 (Wen and Kasper, 1989; Lazaridis *et al.*, 1998; Friess and Yadigaroglu, 2002).

Fig. 8 presents the fractional resuspension rate versus time for each layer of a 3-layer deposit and plotted at different friction velocities. Using Eq. (17) to fit the numerical results of the model, values for ε were derived. Table 2 presents
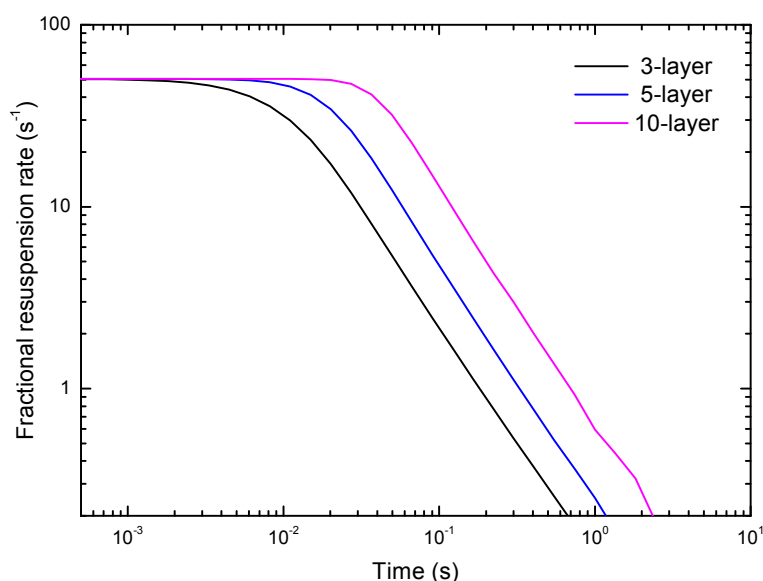
Fig. 7. Total fractional resuspension rate for a 3-layer, a 5-layer and a 10-layer deposit composed of 60 stainless steel particles on a stainless steel surface versus time at friction 0.4 m s^{-1}. The *FY* kinetic was used.
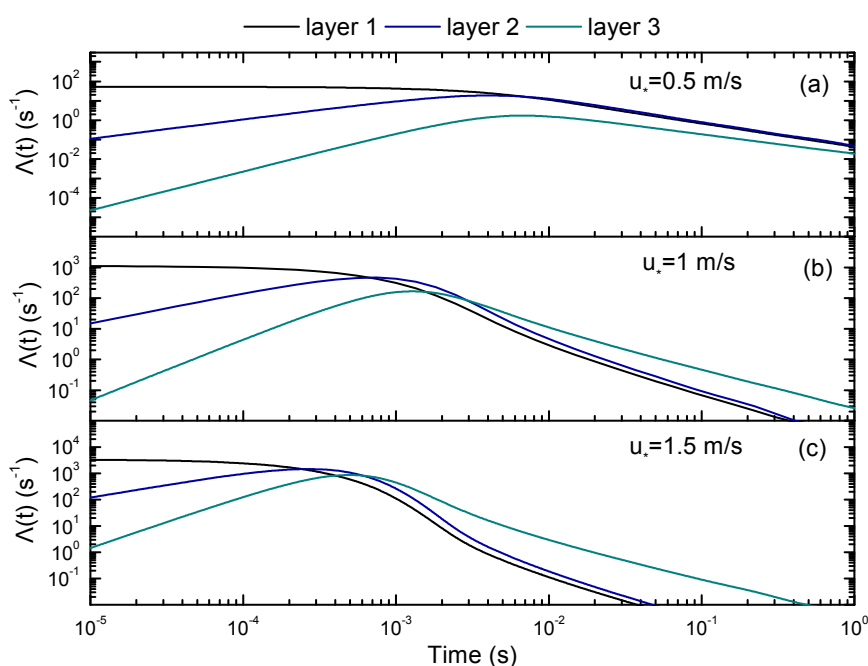
Fig. 8. Fractional resuspension rate for each layer of a 3-layer deposit of 30 μm stainless steel particles on a stainless steel surface versus exposure time at different friction velocities. The *LD* kinetic was used.

Table 2. Fitted values for the decay constant using Eq. (17) for each friction velocity in Fig. 8.

Friction velocity, m s^{-1}	ε		
	Layer 1	Layer 2	Layer 3
0.5	1.167	1.155	1.002
1	1.710	1.686	1.372
1.5	1.829	1.805	1.547

the fitted values of ε applied in Eq. (17) for each friction velocity and layer. Our numerical results confirm the power law, although, the values of ε were scattered and usually

above 1. Values higher than 1 are also reported in Benito *et al.* (2015). Hence, the present results indicate that the long-term fractional resuspension rate decays inversely with

exposure time but with rates higher than the $1/t$ law. Table 2 also suggests that ε increases with friction velocity for all layers. We found that the decay constant ε increases linearly with friction velocity. The linear increase of ε with friction velocity is associated with enhanced decrease of the fractional resuspension rate at higher friction during long exposures. In other words, a higher ε corresponds to a stronger removal force therefore the slope of the curves maintain higher estimates. A similar characteristic is reported in Benito *et al.* (2015), where the behaviour of the resuspension flux at long-term regime was associated with the degree of the overlap between the aerodynamic and the adhesive force distributions.

In addition, Fig. 8 suggests an inverse of the curves at long-term regime. At short exposure time higher resuspension rates correspond to the layers closer to the flow, $\Lambda_1(t) > \Lambda_2(t) > \Lambda_3(t)$, as a direct consequence of the position of the layer. Particles at layer 1 resuspend with the highest rates since there is no obstacle from above. However, at long-term regime when resuspension has moved further into the deposit this behaviour is inversed and $\Lambda_3(t) > \Lambda_2(t) > \Lambda_1(t)$. Model predictions suggest that more particles detach from bottom layer (expressed by the higher rates), since particles at layer 1 and 2 were resuspended prior to particles at layer 3. Thus $\Lambda(t)$ decreases faster at these two layers. This observation is not clearly shown in Fig. 8(a) (as well as in Fig. 6), but this is due to the decreased removal force represented by $u_* = 0.5$ m s^{-1}, where longer exposure to the flow is needed to obtain the inverse of the curves.

Influence of Friction Velocity

Fig. 9(a) presents the influence of friction velocity on the fractional resuspension rate, where, $\Lambda(t)$ is evaluated using three deposits that differ only on the number of the layers. It is seen that $\Lambda(t)$ increases with u_* for low friction velocities but the opposite behaviour is observed for high friction velocities. Again, we distinguish two regimes one corresponding at low friction velocities and one corresponding at high friction velocities. Accordingly, at low-friction regime, particles resuspend with higher rates for higher friction due to the enhanced aerodynamic forces represented herein by the friction velocity. On the other hand, at high-friction regime $\Lambda(t)$ decreases with u_* since the amount of adhered particles within the deposit becomes much less than the initially deposited and the resuspension rate decreases gradually. In fact, the inset in Fig. 9(a) indicates that peak resuspension rate corresponds to 0.5 fraction remaining for all three deposits. After that point the remaining fraction of particles is less than 50%, i.e., more particles have entrained to the air than lying within the deposit. Eventually, all particles become resuspended and $\Lambda(t)$ reaches zero values.

In agreement with the results presented in Fig. 7, higher $\Lambda(t)$ was obtained from the 10-layer deposit as a result of particle resuspension from layers located at $i > 5$ initiated at 0.4 m s^{-1}. Similarly, the 5-layer deposit presents higher rates than the 3-layer deposit due to particle resuspension from layers $i > 3$.

Moreover, Fig. 9(b) plots $\Lambda(t)$ for each discrete layer of the 5-layer deposit presented in Fig. 9(a). The two regimes are indentified for all 5 layers, where at low-friction regime higher rates were obtained for layer 1 followed gradually by the rest four layers according to their position in the deposit. However, at high-friction regime the opposite behaviour is observed and an inverse of the curves takes place. Fig. 9(b) shows that layer 5 preserves greater $\Lambda(t)$ indicating that entrainment is dominated by particle resuspension from this layer. The remaining amount of particles available for resuspension in layer 5 is higher compared to the rest four layers, thus higher rates were obtained. On the other hand, particle entrainment from the layers 1–4 is easier due to their location in the deposit (closer to the top layer) and reduced rates were obtained as a result of less particles adhered within these layers.

CONCLUSIONS

A model based on a stochastic description of particle resuspension was used to evaluate single-layer resuspension rates from multilayer deposits for a range of exposure times and friction velocities. The model determines the particle resuspension from each layer by using a set of kinetic equations to describe the time evolution of resuspension for each individual layer. Two kinetics were applied, one proposed by Lazaridis and Drossinos (1998) and the other proposed by Friess and Yadigaroglu (2001), in which the kinetic equations differ only in their expression for the fraction of particles exposed to the flow.

The numerical results of the present study imply minimal differences when the two kinetics are applied to a 3-layer deposit. It was demonstrated that the higher fraction of exposed particles obtained by the *LD* kinetic results in increased resuspension rates compared to the *FY* kinetic only during short exposures to the airflow. On the contrary, during long exposures, no difference was observed, and no impact on the friction velocity was found, when comparing the two kinetics.

An investigation of the influence of exposure time and friction velocity on the resuspension rates confirmed the existence of two regimes in both cases. Model predictions suggest a time dependence for particle resuspension: High rates apply to a short exposure (short-term regime), whereas considerably reduced rates following a power law are found in a long-term regime. The two regimes were associated with the adhesive forces. In more detail, in the short-term regime, all weakly bound particles resuspend instantaneously—thus, high rates are obtained—whereas in the long-term regime, only the strongly adhered particles remain in the deposit, resulting in substantially reduced rates. Regarding the dependence of $\Lambda(t)$ on friction, the results demonstrate that the resuspension rate increases with u_* in the low-friction regime due to the corresponding enhanced aerodynamic forces, whereas the gradual decrease of $\Lambda(t)$ observed in the high-friction regime is linked to the amount of particles remaining in the deposit (i.e., fewer particles result in lower rates).

In addition, an inverse of the curves of the single-layer resuspension rates was obtained for long-term and high-
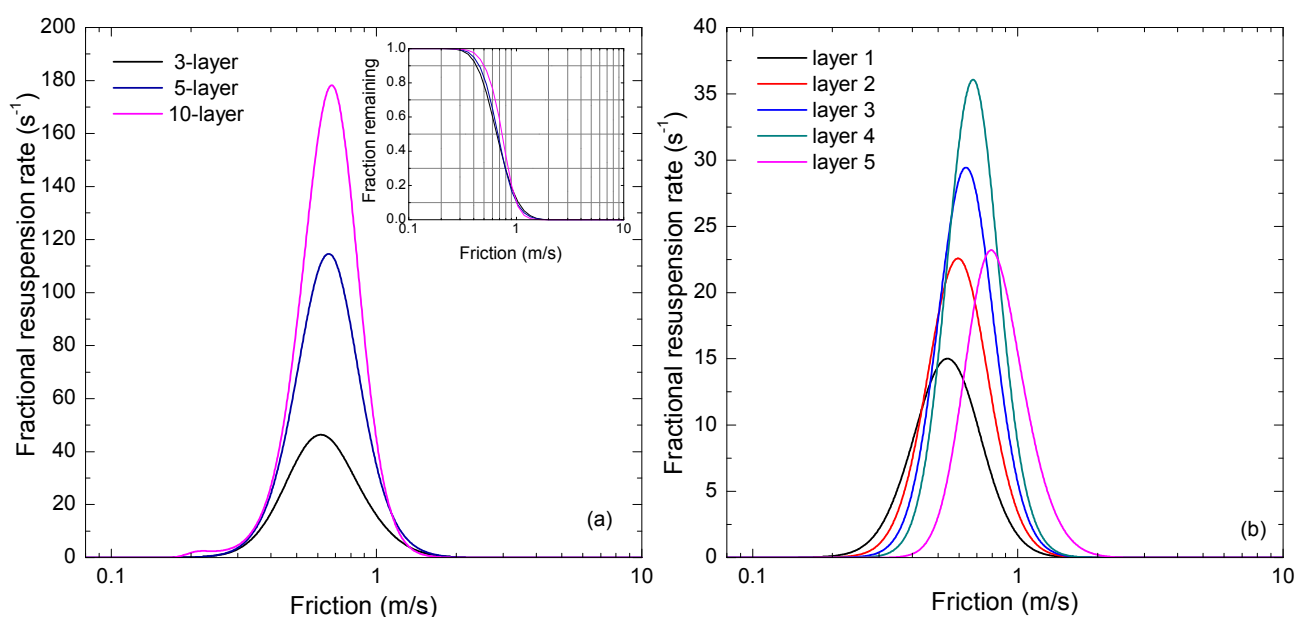
Fig. 9. Fractional resuspension rate of 40 μm stainless steel particles on a stainless steel surface at $t = 0.01\ s$. (a) Effect of friction velocity for a 3-layer, a 5-layer and a 10-layer deposit. The inset corresponds to the corresponding fraction remaining for each deposit and (b) Effect of friction velocity in each discrete layer for a 5-layer deposit.

friction regimes. This behaviour was associated in both cases with the growth of resuspension within the deposit and the relevant dominant layer. Under these circumstances, it was demonstrated that the position of the layer within the deposit plays an important role in the evolution of the process both in terms of a long exposure to the flow, and enhanced aerodynamic forces.

ACKNOWLEDGMENTS

REFERENCES

Barth, T., Reiche, M., Banowski, M., Oppermann, M. and Hampel, U. (2013). Experimental investigation of multilayer particle deposition and resuspension between periodic steps in turbulent flows. *J. Aerosol Sci.* 64: 111–124.

Benito, J.G., Valenzuela Aracena, K.A., Uñac, R.O., Vidales, A.M. and Ippolito, I. (2015). Monte Carlo modelling of particle resuspension on a flat surface. *J. Aerosol Sci.* 79: 126–139.

Boor, B.E., Siegel, J.A. and Novoselac, A. (2013a). Monolayer and multilayer particle deposits on hard surfaces: Literature review and implications for particle resuspension in the indoor environment. *Aerosol Sci. Technol.* 47: 831–847.

Boor, B.E., Siegel, J.A. and Novoselac, A. (2013b). Wind tunnel study on aerodynamic particle resuspension from monolayer and multilayer deposits on linoleum flooring and galvanized sheet metal. *Aerosol Sci. Technol.* 47:

848–857.

Chatoutsidou, S.E., Drossinos, Y., Tørseth, H. and Lazaridis, M. (2017). Modelling of particle resuspension by a turbulent airflow and the role of particle size, surface roughness and electric charge. *J. Adhes. Sci. Technol.* 31: 817–843.

Friess, H. and Yadigaroglu, G. (2001). A generic model for the resuspension of multilayer aerosol deposits by turbulent flow. *Nucl. Sci. Eng.* 138: 161–176.

Friess, H. and Yadigaroglu, G. (2002). Modeling of the resuspension of particle clusters from multilayer aerosol deposits with variable porosity. *J. Aerosol Sci.* 33: 883–906.

Fromentin, A. (1989). *Particle resuspension from a multilayer deposit by turbulent flow*. Ph.D. thesis. Swiss Federal Institute of Technology, Zurich.

Goldasteh, I., Ahmandi, G. and Ferro, A.R. (2013). Monte Carlo simulation of micron size spherical particle removal and resuspension from substrate under fluid flows. *J. Aerosol Sci.* 66: 62–71.

Guingo, M. and Minier, J.P. (2008). A new model for the simulation of particle resuspension by turbulent flows based on a stochastic description of wall roughness and adhesion forces. *J. Aerosol Sci.* 39: 957–973.

Henry, C. and Minier, J.P. (2014). Progress in particle resuspension from rough surfaces by turbulent flows. *Prog. Energy Combust. Sci.* 45: 1–53.

Ibrahim, A.H., Dunn, P.F. and Brach, R.M. (2003). Microparticle detachment from surfaces exposed to turbulent air flow: Controlled experiments and modelling. *J. Aerosol Sci.* 34: 765–782.

Lazaridis, M. and Drossinos, Y. (1998). Multilayer resuspension of small identical particles by turbulent flow. *Aerosol Sci. Technol.* 28: 548–560.

Lazaridis, M., Drossinos, Y. and Georgopoulos, P.G. (1998). Turbulent resuspension of small Nonderfomable Particle. *J. Colloid Interface Sci.* 204: 24–32.

Lecrivain, G., Vitsas, A., Boudounis, A.G. and Hampel, U. (2014). Simulation of multilayer particle resuspension in an obstructed channel flow. *Powder Technol.* 263: 142–150.

Leighton, D. and Acrivos, A. (1985). The lift on a small sphere touching a plane in the presence of a simple shear flow. *J. Appl. Math. Phys.* 36: 174–178.

Mukai, C., Siegel, G.A. and Novoselac, A. (2009). Impact of airflow characteristics on particle resuspension from indoor surfaces. *Aerosol Sci. Technol.* 43: 1022–1032.

O'Neil, M.E. (1968). A sphere in contact with a plane wall in a slow linear shear flow. *Chem. Eng. Sci.* 23: 1293–1298.

Reeks, M.D. and Hall, D. (2001). Kinetic models for particle resuspension in turbulent flows: Theory and measurement. *J. Aerosol Sci.* 32: 1–31.

Reeks, M.W., Reed, J. and Hall, D. (1988). On the resuspension of small particles by a turbulent flow. *J. Phys. D* 21: 574–589.

Stempniewicz, M.M., Komen, E.M.J. and de With, A. (2008). Model of particle resuspension in turbulent flows. *Nucl. Energy Des.* 238: 2943–2959.

Wang, S., Zhao, B., Zhou, B and Tan, Z. (2012). An experimental study on short-time particle resuspension from inner surfaces of straight ventilation ducts. *Build. Environ*. 53: 119–127.

Wen, H.Y. and Kasper, G. (1989). On the kinetics of particle re-entrainment from surfaces. *J. Aerosol Sci.* 20: 483–498.

Wu, Y.L., Davidson, C.I. and Russell, A.G. (1992). Controlled wind tunnel experiments for particle bounceoff and resuspension. *Aerosol Sci. Technol.* 17: 245–262.

Zhang, F., Reeks, M.W., Kissane, M.P. and Perkins, R.J. (2013). Resuspension of small particles from multilayer deposits in turbulent boundary layers. *J. Aerosol Sci.* 66: 31–61.

Zhou, B., Zhao, B. and Tan, Z. (2011). How particle resuspension from inner surfaces of ventilation ducts affects indoor air quality-A modelling analysis. *Aerosol Sci. Technol.* 45: 996–1009.

Ziskind, G., Fichman, M. and Gutfinger, C. (1995). Resuspension of particulates from surfaces to turbulent flows-Review and analysis. *J. Aerosol Sci.* 26: 613–644.

Ziskind, G., Fichman, M. and Gutfinger, C. (1997). Adhesion moment model for estimating particle detachment from a surface. *J. Aerosol Sci.* 28: 623–634.

Ziskind, G. (2006). Particle resuspension from surfaces: Revisited and re-evaluated. *Rev. Chem. Eng.* 22: 1–123.